forests

MDPI

Article

Assessing Spring Phenology Models with Photosynthesis Integration: Mechanistic Drivers of the Carbon–Frost Trade-Off

Yating Gu [1], Qianhan Wu [2], Xiaorong Wang [2] and Yantian Wang [3,*]

[1] Jiangsu Key Laboratory of Soil and Water Processes in Watershed, College of Geography and Remote Sensing, Hohai University, Nanjing 211100, China; yatinggu@hhu.edu.cn
[2] Research Area of Ecology and Biodiversity, School of Biological Sciences, The University of Hong Kong, Hong Kong 999077, China; qhwu@connect.hku.hk (Q.W.); xrwang@connect.hku.hk (X.W.)
[3] NARI Group Corporation State Grid, Electric Power Research Institute, Nanjing NARI Information Communication Technology Co., Ltd., Nanjing 211106, China
* Correspondence: wangyantian@sgepri.sgcc.com.cn

Abstract

Accurate prediction of spring phenology is critical for understanding ecosystem carbon and water dynamics under changing climates. In this study, we applied a revised optimality-based model (R-OPT) that integrates a mechanistic photosynthesis framework into the existing OPT model to simulate leaf unfolding date. We evaluated R-OPT alongside three widely used models—Growing Degree Days (GDD), Chilling–Forcing Trade-off (CFT), and Optimality-based (OPT) models—across multiple Plant Functional Types (PFTs) and sites using repeated 5-fold cross-validation. Findings reveal that R-OPT consistently outperforms the other models, achieving the lowest median RMSE (13.11 days), indicating enhanced predictive accuracy and explanatory power. Although the model incurs slightly higher complexity (median AIC = 13.44), the improvement in prediction justifies the trade-off. Our results highlight the importance of incorporating plant functional traits and environmental heterogeneity in phenological modeling. PFT-specific differences, such as the lower RMSEs for evergreen forbs and deciduous broadleaf PFTs versus larger uncertainties for drought-deciduous and semi-evergreen PFTs, underscore that current models may insufficiently capture key environmental drivers, including precipitation and partial leaf retention. Latitudinal and elevational variations in trade-off parameter a, and the prominence of leaf-level carbon assimilation traits (Aleaf) as drivers of phenology, demonstrate the critical role of physiological traits in shaping PFT-specific phenological timing. These findings have significant implications for large-scale ecosystem modeling. By linking phenology directly to photosynthetic processes, R-OPT enhances predictive skill and biological interpretability, supporting improved simulations of carbon and water fluxes. Overall, R-OPT offers a mechanistically grounded and robust framework for advancing predictive understanding of spring phenology and its ecological and climate-relevant consequences.

Keywords: spring phenology; photosynthesis framework; carbon gain; chilling risk; Earth System Models

Check for updates

Academic Editors: Romà Ogaya and Jiaxin Wang

Received: 26 December 2025
Revised: 14 February 2026
Accepted: 17 February 2026
Published: 23 February 2026

Copyright: © 2026 by the authors. Licensee MDPI, Basel, Switzerland. This article is an open access article distributed under the terms and conditions of the Creative Commons Attribution (CC BY) license.

1. Introduction

Spring phenology—the timing of biological events such as leaf-out, flowering, and budburst—plays a critical role in regulating ecosystem structure and function [1]. It marks the onset of the growing season, influencing carbon uptake, water use, and energy exchange between the land surface and atmosphere [2–4]. Shifts in spring phenology can alter

agricultural productivity, forest dynamics, and the global carbon cycle [5–7]. Understanding the mechanisms and consequences of phenological changes is therefore essential for predicting ecosystem responses to ongoing and future climate variability [8–10].

Over the past few decades, research on spring phenology has progressed from simple empirical observations to process-based modeling that only considers abiotic factors, such as one-phase models like the Growing Degree Days model and the Sequential model. To specify, temperature-driven one-phase models, such as the Growing Degree Day (GDD) approach, assume that leaf emergence occurs once cumulative heat accumulation surpasses a threshold [11,12]. Although these kinds of models are quite straightforward, they tend to oversimplify the physiological processes behind phenological transitions, leading to systematic biases across Plant Functional Types (PFTs) and regions [13]. Secondly, two-phase models offer improvement by recognizing that both winter chilling and spring forcing jointly control the leaf unfolding date [14,15]. However, they rely heavily on empirical, PFT-specific parameters, and there is still uncertainty regarding how these two processes interact [16–18]. More recently, optimality-based (OPT) models, which link plant physiological mechanisms with ecosystem dynamics, have reframed phenology as an adaptive trade-off between maximizing photosynthetic gain and minimizing frost damage risk, providing a more mechanistic and flexible framework for predicting vegetation's responses to climate change [19,20].

There is increasing recognition that optimality-based (OPT) approaches provide a more realistic framework for modeling spring phenology, as they capture the adaptive balance between maximizing carbon gain and minimizing frost risk [9,21]. These models have shown strong predictive capability across diverse ecosystems when compared with traditional temperature- or threshold-based approaches. In a previous study [20], the research assumed globally uniform values of Vcmax and Jmax, rather than accounting for their spatial and PFT-level variability, which can affect plant photosynthesis rates. Also, significant residual errors remain in previous studies (errors in 16% of the Northern Hemisphere of more than 10 days; Gu et al., 2025), suggesting that key physiological and environmental mechanisms of the potential photosynthesis gain before the leaf unfolding date are still missing [19,22]. If spring phenology is indeed governed by a trade-off between photosynthetic benefit and chilling damage, then incorporating processes that directly influence carbon assimilation could improve model performance beyond what is achievable with simple photoperiod or temperature forcing functions [23,24]. The coupled Farquhar–Medlyn model, which integrates biochemical photosynthesis and stomatal conductance processes, offers a promising way forward [25–27]. By explicitly representing environmental drivers such as temperature, humidity, CO_2 concentration, and atmospheric pressure, this framework allows for a more mechanistic connection between phenology and photosynthetic activity [28]. Integrating such models into phenological prediction could provide a stronger physiological basis for assessing vegetation responses under future climate scenarios [8,29].

The growing availability of long-term observational datasets—from both ground-based monitoring networks and crowd-sourced efforts—now provides an ideal opportunity to evaluate ecosystem-level phenology models and their underlying mechanisms. Ground observations, when combined with statistical modeling techniques, allow us to generate key environmental variables (such as temperature, vapor pressure deficit, and shortwave radiation in the Daymet dataset) at fine spatial resolution; for example, on a 1 km $\times$ 1 km grid [30]. At the same time, the USA National Phenology Network contributes rich, continuous time-series records collected by thousands of volunteer observers and partner organizations at the organism scale [31,32]. Together, ecosystem-scale environmental measurements and labor-intensive organism-level phenology observations offer

a reliable foundation for testing and refining phenology models [33,34]. As a result, the mechanisms embedded in these models become more transparent and easier to interpret.

This study examines whether existing models of spring phenology adequately capture the underlying physiological mechanisms needed to interpret vegetation responses to environmental variability and anticipate future changes under a warming climate. To address this, we evaluated four process-based models—Growing Degree Days (GDD), Chilling–Forcing Trade-off (CFT), an Optimality-based (OPT) model, and a revised optimality-based model coupling the carbon assimilation process (R-OPT)—using the USA-NPN phenology dataset. We further employed a random forest algorithm to identify the relative importance of environmental drivers, assessing whether variables associated with leaf photosynthetic activity contribute to phenological prediction beyond temperature effects for parameter α. This is because the plants need to endure chilling and then accept forcing to unfold their leaves, and α is just the parameter balancing the chilling and forcing/potential photosynthesis gain requirement. Our specific objectives were: (1) to compare the performance of traditional temperature- and chilling-based models (GDD and CFT) with optimality-based frameworks (OPT and R-OPT); (2) to test the consistency of model performance across different temperate tree PFTs: forbs, deciduous broadleaf forests, evergreen broadleaf forests; and (3) to investigate the relative importance of environmental and physiological factors that determine the trade-off parameter α in the carbon gain-frost damage balance.

2. Materials and Methods

2.1. Study Area

The study area for this research covers the continental United States, extending approximately across latitudes 25–50° N and longitudes 65–125° W, encompassing a wide range of climatic and ecological regions (Figure 1). In this study, we mainly focused on five plant functional types: deciduous broadleaf (DB), evergreen broadleaf (EB), semi-evergreen broadleaf (SEB), evergreen forb (EF), and drought-deciduous broadleaf (DDB). Elevations range from near sea level along the coasts to over 2500 m in major mountain ranges such as the Rockies and Appalachians [35]. This region was selected for two main reasons: (1) the USA-NPN dataset provides extensive, high-quality, open-access records of key phenophases—including leaf-out, flowering, and fruiting—enabling robust evaluation of phenology models across multiple PFTs and decades; and (2) the broad gradients in latitude, longitude, climate, topography, and vegetation types offer sufficient environmental variability to test model performance and evaluate the applicability of mechanistic and optimality-based approaches across diverse temperate ecosystems. Study sites were selected from the USA National Phenology Network (US-NPN) based on the following criteria. First, observations were restricted to the plant kingdom (*Plantae*) and the phenophase category *Leaves*. Second, we included multiple plant functional types, including deciduous broadleaf, drought-deciduous broadleaf, evergreen broadleaf, semi-evergreen broadleaf, and evergreen forb PFTs. Finally, only records corresponding to the phenophase *Breaking leaf buds* were retained for analysis.

2.2. Materials

This study integrates multiple datasets to examine spring phenology optimality strategies across different plant functional types (PFTs). Leaf unfolding dates were obtained from the USA-National Phenology Network (NPN) database (https://www.usanpn.org/; accessed on 1 December 2025), which has provided open-source PFT-level observations across the United States since 1958. Climate data were sourced from Daymet (https://daymet.ornl.gov/; accessed on 1 December 2025), offering high-resolution daily records, while leaf photosynthetic capacity (Vcmax) was included from [36]. Long-

term atmospheric CO_2 trends were incorporated using Mauna Loa Observatory data (https://gml.noaa.gov/data/data.php?parameter_name=Carbon+Dioxide&site=MLO; accessed on 1 December 2025). Together, these datasets enable a mechanistic analysis of the environmental and physiological drivers of phenology.

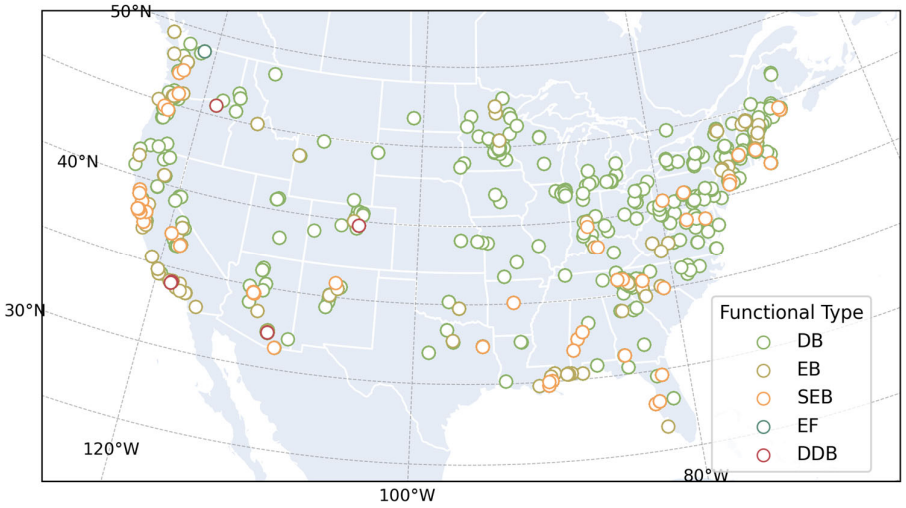


Figure 1. Distribution of study sites within the US-NPN. This study focuses on five plant functional types with broad spatial coverage and abundant phenological observations: evergreen forb (EF), evergreen broadleaf (EB), semi-evergreen broadleaf (SEB), deciduous broadleaf (DB), and drought-deciduous broadleaf (DDB). These PFT groups are widely distributed across the United States.

2.2.1. Phenological Data

This study draws on long-term, ground-based observations of spring phenology across different plant functional types (PFTs), focusing on key events such as leaf unfolding date (LUD). These data were sourced from the USA-NPN database, which has systematically recorded PFT-level phenological dates across the United States since 1958, providing a rich resource for evaluating temporal trends and testing predictive models. Firstly, the *Kingdom* was chosen as *Plantae* and the *Phenophase_ID* was selected as *Leaves*; secondly, we selected several plant functional types, which were deciduous broadleaf, drought-deciduous broadleaf, evergreen broadleaf, evergreen forb, semi-evergreen broadleaf; thirdly, the *Phenophase_Description* was selected as *Breaking leaf buds*.

2.2.2. Environmental Data

Climate and environmental drivers were compiled from multiple sources. Daily meteorological data, including temperature, precipitation, and solar radiation, were obtained from Daymet, which provides high-resolution (~1 km) gridded climate data across the United States, and we used the US-NPN selected sites' longitude and latitude to extract the ecosystem-level nearest 1 km grid's weather data. Leaf photosynthetic capacity (Vcmax) was included from [36] using Rstudio 2024.09.1 readMat, and long-term atmospheric CO_2 concentrations were taken from the Mauna Loa Observatory. By matching each phenological site to its corresponding Daymet grid cell based on latitude and longitude, we ensured that local climate conditions were accurately represented for model simulations, supporting the analysis of how environmental variables influence spring phenology.

2.3. Data Analysis

In this study, we developed a novel spring phenology model (R-OPT) that combines the optimality-based principle, as employed in Meng et al. (2021) [37], with a process-based photosynthesis model, specifically the coupled Farquhar–Medlyn photosynthesis model [20]. Model performance was assessed using the US-NPN benchmark phenology

dataset and systematically compared against three established prognostic models: the Growing Degree Day (GDD) model, the Chilling–Forcing Trade-off (CFT) model, and the original Optimality-based (OPT) model. This analytical framework enabled a rigorous evaluation of R-OPT and clarified the conditions under which it provides demonstrable advantages relative to existing approaches.

2.3.1. Prognostic Phenology Models

We evaluated four distinct phenological models, outlining their specific formulations and the theoretical assumptions below:

In the first model, leaf-out is triggered when sufficient warmth has accumulated. Specifically, the model determines the leaf-out date as the first day on which cumulative growing degree days exceed the defined heat requirement.

$$R_{f,i} = \begin{cases} 0, & T_i \leq T_{base} \\ T_i - T_{base} & T_i > T_{base} \end{cases} \quad (1)$$

$$F_t = \sum_{i=t_0}^{t} R_{f,i} \quad (2)$$

The model assumes a base temperature of 5 °C, below which no forcing accumulates. Daily forcing rates $R_{f,i}$ are integrated beginning on day t_0 to produce the cumulative forcing F_t. Budburst is deemed to occur when this cumulative value satisfies the threshold condition $F_t \geq F_{\text{thres}}$ (Equation (2)).

The CFT approach integrates two temperature-mediated processes—chilling and forcing—to regulate leaf-out. Both accumulate beginning in winter, and spring budburst is assumed to occur only when forcing outpaces a threshold modulated by accumulated chilling. Chilling is quantified via a triangular temperature response, whereas forcing follows a sigmoidal response (Equations (3)–(6)).

$$R_{c,i} = \begin{cases} 0 & T_i < T_{min} \\ \frac{T_i - T_{min}}{T_{opt} - T_{min}} & T_{min} \leq T_i < T_{opt} \\ \frac{T_i - T_{opt}}{T_{max} - T_{opt}} & T_{opt} \leq T_i < T_{max} \\ 0 & T_i > T_{max} \end{cases} \quad (3)$$

$$R_{f,i} = \begin{cases} 0, & T_i \leq T_{base} \\ \frac{28.4}{1+\exp(3.4-0.185T_i)} & T_i > T_{base} \end{cases} \quad (4)$$

$$C_t = \sum_{i=t_0}^{t} R_{c,i} \quad (5)$$

$$F_t = \sum_{i=t_0}^{t} R_{f,i} \quad (6)$$

The variable T_i denotes average temperature on day i, with the minimum, optimal, and maximum temperatures for the response functions fixed at −5 °C, 10 °C, and 25 °C [38]. For each day, the model computes a forcing increment $R_{f,i}$ and a chilling increment $R_{c,i}$. Their accumulated totals (F_t and C_t) are obtained by summing from the beginning of the calendar year (1 January). Two parameters, a and b, determine how chilling adjusts the amount of forcing required for budburst. Leaf-out occurs when the accumulated forcing exceeds the chilling-modified threshold ae^{-bC_t}, representing the interplay between winter cooling and spring warming in regulating phenological development.

Building upon CFT, the OPT model introduces an additional component—a photoperiod response that depends on accumulated chilling [37]. This structure reflects empirical findings that daylength can amplify or constrain forcing accumulation, especially when winter chilling is insufficient. The model is motivated by the idea that plants regulate leaf-out to maximize early carbon assimilation while avoiding the hazards associated with inadequate chilling. Model formulation is presented in Table 1 (Equations (7)–(11)).

$$R_{c,i} = \begin{cases} 0 & T_i < T_{min} \\ \frac{T_i - T_{min}}{T_{opt} - T_{min}} & T_{min} \le T_i < T_{opt} \\ \frac{T_i - T_{opt}}{T_{max} - T_{opt}} & T_{opt} \le T_i < T_{max} \\ 0 & T_i > T_{max} \end{cases} \quad (7)$$

$$R_{f,i} = \begin{cases} 0, & T_i \le T_{base} \\ \frac{28.4}{1+\exp(3.4-0.185T_i)} & T_i > T_{base} \end{cases} \quad (8)$$

$$R_{p,i} = \frac{L_i}{12} e^{-cR_{c,i}} \quad (9)$$

$$C_t = \sum_{i=t_0}^{t} R_{c,i} \quad (10)$$

$$F_t = \sum_{i=t_0}^{t} R_{f,i} \times R_{p,i} \quad (11)$$

Table 1. Summary of study sites.

PFTs	NO of Records	Temporal Range	Elevation Range (m)	Climate Data Included
Deciduous Broadleaf	17,477	2007–2023	0–3385	Yes
Drought-Deciduous Broadleaf	49	2009–2014	34–2087	Yes
Evergreen Broadleaf	1437	2009–2023	0–2796	Yes
Evergreen Forb	56	2011–2016	311–409	Yes
Semi-evergreen Broadleaf	506	2011–2023	0–2216	Yes

The variable T_i represents the daily mean temperature, and the lower, optimal, and upper temperature limits (−5 °C, 10 °C, 25 °C) are adopted from [38]. For each day, the model calculates forcing ($R_{f,i}$), chilling ($R_{c,i}$), and realized forcing ($R_{p,i}$) according to Meng et al. (2021) [37], as well as the corresponding daylength L_i (detailed calculation methods can be found in Supplementary Materials). Summing these daily contributions from the start of the calendar year (1 January) gives cumulative chilling C_t and forcing F_t. The parameters a, b, and c regulate the sensitivity to chilling and photoperiod. Leaf-out is assigned to the first day when realized forcing (Equation (11)) reaches the threshold ae^{-bC_t}, marking the point at which expected carbon assimilation benefits outweigh potential frost-related costs.

The fourth model, referred to as the revised OPT (R-OPT), represents an extension of the original OPT framework with two key advances. First, it preserves the central premise of the OPT model—that spring phenology emerges from a balance between frost-related chilling risk (Equations (12) and (13)) and the benefits of early-season carbon uptake (Equation (14)–(16)). Second, instead of relying on photoperiod-based adjustments to forcing efficiency (as in Meng et al., 2021) [37], the R-OPT model introduces a mechanistic representation of photosynthesis. By incorporating a process-based photosynthesis module, the model can more realistically describe potential carbon gain and explicitly account for

additional environmental drivers such as radiation, CO_2 concentration, and atmospheric moisture, all of which have been recognized as important determinants of spring phenological responses [19,39]. To simulate potential photosynthetic carbon assimilation, we employed the coupled Farquhar [40]–Medlyn [41] photosynthesis–stomatal conductance model using daily meteorological inputs (Equation (14)). This coupled model has been widely validated and shown to capture observed patterns of photosynthetic behavior across diverse ecosystems. The resulting formulation allows R-OPT to directly evaluate how variability in potential carbon gain modulates the timing of leaf-out.

$$R_{c,i} = \begin{cases} 0 & T_i < T_{min} \\ \frac{T_i - T_{min}}{T_{opt} - T_{min}} & T_{min} \le T_i < T_{opt} \\ \frac{T_i - T_{opt}}{T_{max} - T_{opt}} & T_{opt} \le T_i < T_{max} \\ 0 & T_i > T_{max} \end{cases} \quad (12)$$

$$C_t = \sum_{i=t_0}^{t} R_{c,i} \quad (13)$$

$$R_{f,i} = Photosyn(A_n, g_s) \quad (14)$$

$$R_{p,i} = \frac{L_i}{12} e^{-cR_{c,i}} \quad (15)$$

$$F_t = \sum_{i=t_0}^{t} R_{f,i} \times R_{p,i} \quad (16)$$

Within the R-OPT framework, T_i denotes the mean temperature on day i, while the temperature bounds $T_{\text{min}} = -5\ ^\circ C$, $T_{\text{opt}} = 10\ ^\circ C$, and $T_{\text{max}} = 25\ ^\circ C$, following [38]. The model computes a daily photosynthetic potential $R_{f,i}$, a chilling rate $R_{c,i}$, and a realized forcing term $R_{p,i}$ (Meng et al., 2021) [37]. Accumulated chilling and photosynthetic forcing from the start of the calendar year (t_0 was set as 1 January) to day t are denoted by C_t and F_t, respectively. Three parameters—a, b, and c—are calibrated for the model. Leaf-out is predicted for the first day i on which accumulated realized forcing for potential carbon assimilation F_t (Equation (16)) reaches or exceeds the chilling-dependent requirement ae^{-bC_t}. In essence, the model identifies leaf-out as the moment when the anticipated carbon gain outweighs the frost-related constraints imposed by insufficient chilling.

This $R_{f,i} = \text{Photosyn}(A_n, g_s)$ framework (Equation (14)) computes net leaf photosynthesis by jointly accounting for environmental controls using RStudio 2024.09.1 Photosyn function, with the photosynthetic rate determined from the hyperbolic minimum of the V_{cmax}-, J_{max}-, and TPU-limited rates. When intercellular CO_2 concentration (C_i) is not prescribed, it is obtained by numerically locating the intersection between CO_2 demand, as defined by the Farquhar model, and CO_2 supply, as governed by the Medlyn stomatal conductance formulation. The complete mathematical expression is given below:

$$A_n = \min(A_c,\ A_j,\ A_p) - R_d \quad (17)$$

$$g_s = g_0 + 1.6 * \left(1 + \frac{g_1}{\sqrt{VPD}}\right) * \frac{A_n}{C_a} \quad (18)$$

In this framework, A_c represents the Rubisco-limited photosynthetic rate and is governed by the maximum carboxylation capacity at a reference temperature of 25 °C ($V_{c,\text{max25}}$, μmol CO_2 m^{-2} s^{-1}). A_j denotes the RuBP regeneration–limited rate, while A_p captures the triose-phosphate utilization (TPU) limitation, both expressed in μmol CO_2 m^{-2} s^{-1}. R_d denotes mitochondrial CO_2 release under light conditions. The stomatal component

includes the residual conductance to water vapor (g_0, mol m^{-2} s^{-1}), vapor pressure deficit (VPD, kPa), stomatal slope (g_1), and atmospheric CO_2 concentration (C_a, ppm).

2.3.2. Model Fitting and Validation

In this study, model training and calibration were performed using a repeated 5-fold cross-validation approach for bias-variance trade-off following, applied individually to each PFT at each site [42].

Model performance was assessed using the root mean squared error (RMSE), with calibration aimed at minimizing discrepancies between simulated and field-observed leaf-out dates (LUD) over the available multi-decadal time series. For each site–PFT combination, annual observations were randomly partitioned at the year level into calibration and independent validation subsets across five folds, and the entire cross-validation procedure was repeated 20 times to reduce sensitivity to individual data partitions.

For each target site–year, predicted LUD values from all repetitions (n = 20) were averaged to obtain an ensemble prediction used in subsequent analyses, rather than relying on a single calibration outcome.

Beyond overall model performance, we conducted site–PFT-level comparisons to quantify relative model improvements. For each model pair, RMSE differences were computed across all site–PFT combinations, and the resulting distributions were analyzed to assess the consistency and magnitude of performance gains.

2.3.3. Random Forest Factor Importance

In this study, because parameter a represents the trade-off between frost damage avoidance and carbon gain in plants, we applied a random forest regression approach to identify the dominant factors constraining this balance. The analysis included AccumChilling, AccumForcing, air temperature, elevation, leaf area (Aleaf), shortwave radiation (SRAD), and vapor pressure deficit (VPD) as predictor variables. The random forest model was trained on a randomly split dataset (75% training, 25% testing), and variable importance was quantified using the mean decrease in impurity metric to assess the relative contribution of each predictor to explaining variability in parameter a.

3. Results

3.1. Evaluation of Model Performance Within and Among Tree PFTs

Across the four prognostic spring phenology models (GDD, CFT, OPT, and R-OPT), our cross-model evaluation demonstrated that R-OPT consistently yielded the highest predictive accuracy among the tested approaches (Figure 2). Based on the median values across all PFTs and sites, R-OPT achieved the lowest RMSE (13.11 days, with 25% Q1 5.89 days and 75% Q3 43.10 days), outperforming OPT (17.75 days, with 25% Q1 6.26 days and 75% Q3 47.01 days), GDD (27.16 days, with 25% Q1 7.06 days and 75% Q3 49.65 days), and CFT (22.12 days, with 25% Q1 6.37 days and 75% Q3 50.91 days) (Figure 2a). Although R-OPT exhibited a somewhat higher median AIC (13.44) compared with GDD (9.71) and CFT (11.61), its improved predictive accuracy and explanatory power suggest a better overall balance between model fit and complexity (Figure 2b). These findings remained consistent across both aggregated and Plant Functional Type (PFT)-specific analyses, reinforcing that the R-OPT model offers the most robust and accurate representation of spring phenological responses among the four models.

Our results in Figure 2c reinforce the interpretation of Figure 2 by providing more rigorous statistical evidence, demonstrating consistent findings across different model performance metrics and analytical levels (PFT-specific and all-PFTs). For instance, the median RMSE of R-OPT was 14.61 days for deciduous broadleaf (DB) PFTs, 56.55 days for deciduous dry

broadleaf (DDB), 52.17 days for evergreen broadleaf (EB), 10.27 days for evergreen forest (EF), and 50.39 days for semi-evergreen broadleaf (SEB). These values were consistently lower than or comparable to those of the other models, confirming that R-OPT provides the most reliable and generalizable predictions of spring phenology across different PFTs.

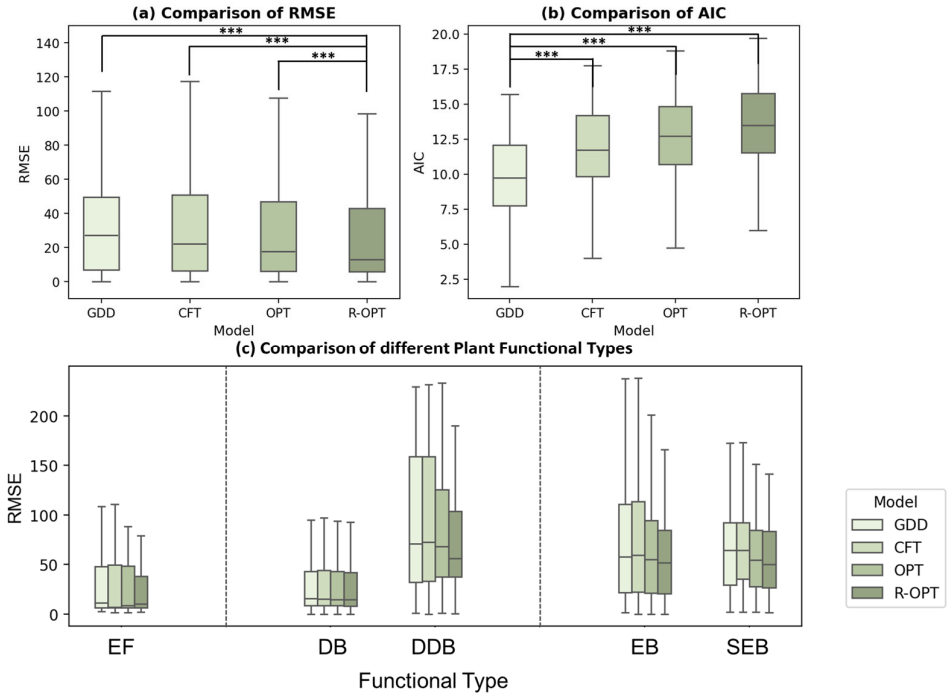


Figure 2. Performance comparison of four prognostic spring phenology models based on 5-fold cross-validation. (**a**) RMSE, (**b**) AIC, and (**c**) RMSE comparisons across different plant functional types (*** denotes p-value < 0.001).

Figure 3 shows the relationship between observed and modeled DOY, with point density indicated by color and the dashed line representing the 1:1 reference. Reported R^2 values correspond to each model–PFT combination. Across all PFTs, R-OPT consistently yields the highest R^2 (Forb: 0.58; Deciduous Broadleaf: 0.40; Evergreen Broadleaf: 0.45), outperforming GDD, CFT, and OPT and better capturing variability in leaf-out timing.

Moreover, analyses across elevation gradients revealed a consistent advantage of R-OPT (Figure 4). Median RMSE values for R-OPT were 13.40 days (0–500 m), 11.07 days (500–1000 m), 19.35 days (1000–1500 m), 14.82 days (1500–2000 m), and 9.90 days (>2000 m). In every elevation group, R-OPT yielded lower errors than the other models, with particularly large improvements observed at higher elevations (>2000 m). Together, these results demonstrate that R-OPT consistently delivers superior predictive performance across environmental gradients and functional groups, underscoring its robustness and generalizability for modeling spring phenology.

3.2. Spatial Analysis of PFT-Level Differences in Paired Model Performance

Building upon the previous histogram-based comparison, we further examined the spatial consistency of performance differences among the four prognostic models across the study region. To achieve this, site-level paired model performance differences (quantified as the difference in RMSE) were categorized into five groups, as shown in Figure 5. Overall, the R-OPT vs. OPT comparison exhibited greater model improvement than the OPT vs. CFT comparison, with enhanced sites more densely distributed along coastal areas. The summary chart in the lower left of Figure 4 further indicates that CFT often performed worse than GDD. For both the OPT–CFT and R-OPT–OPT model pairs, the proportion of sites

showing improvement (i.e., reduced RMSE) exceeded 50% across all vegetation functional types—EF (76.19%), DB (89.95%), DDB (76.19%), EB (85.09%), and SEB (86.42%)—demonstrating the robustness of the R-OPT model across diverse vegetation types (Figure 5c,f,i,l,o).

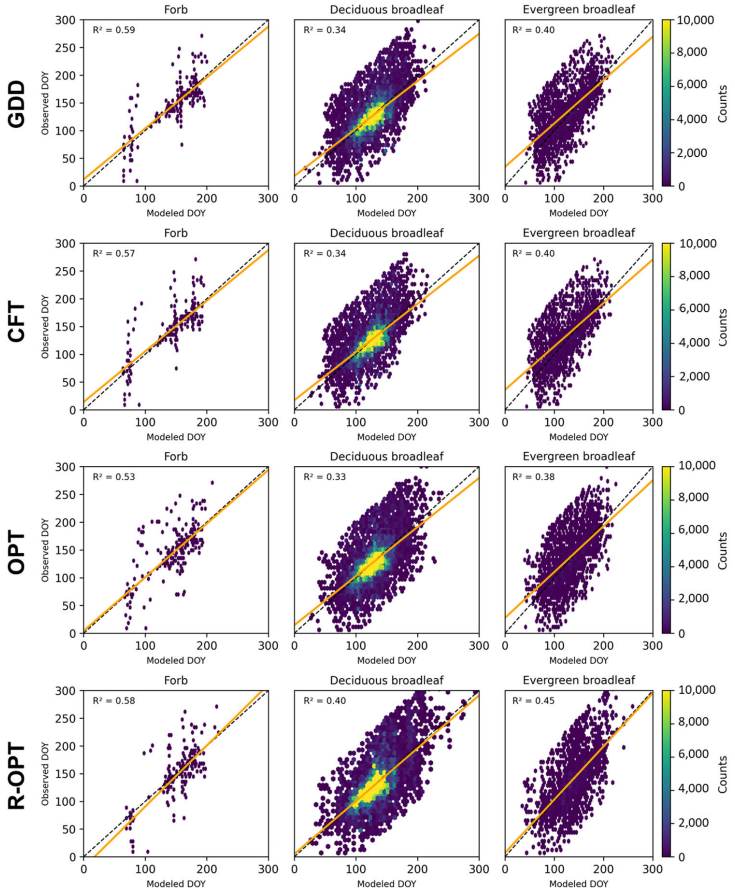


Figure 3. Comparison of modeled versus observed spring leaf-out dates across three plant functional types (forb, deciduous broadleaf, evergreen broadleaf) for four phenology models (GDD, CFT, OPT, and R-OPT).

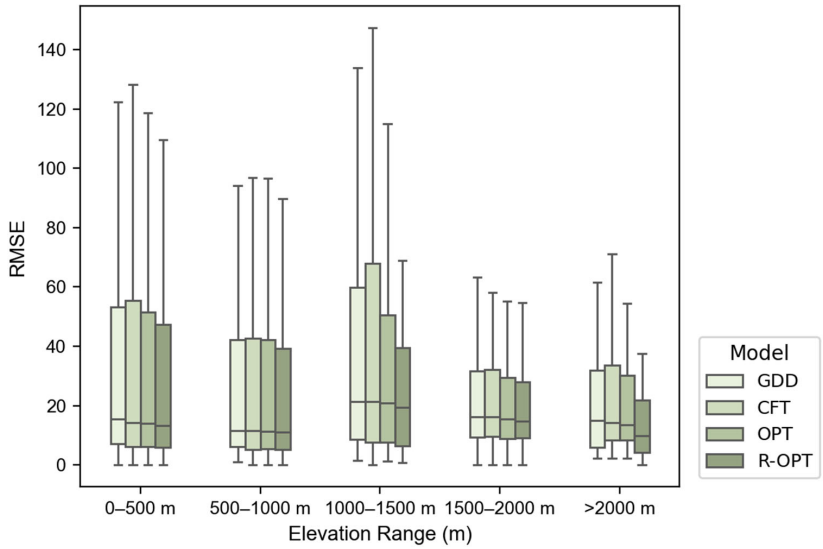


Figure 4. RMSE-based model performance differences across elevation groups. The x-axis represents elevation ranges, and RMSE (in days) indicates differences in model performance.

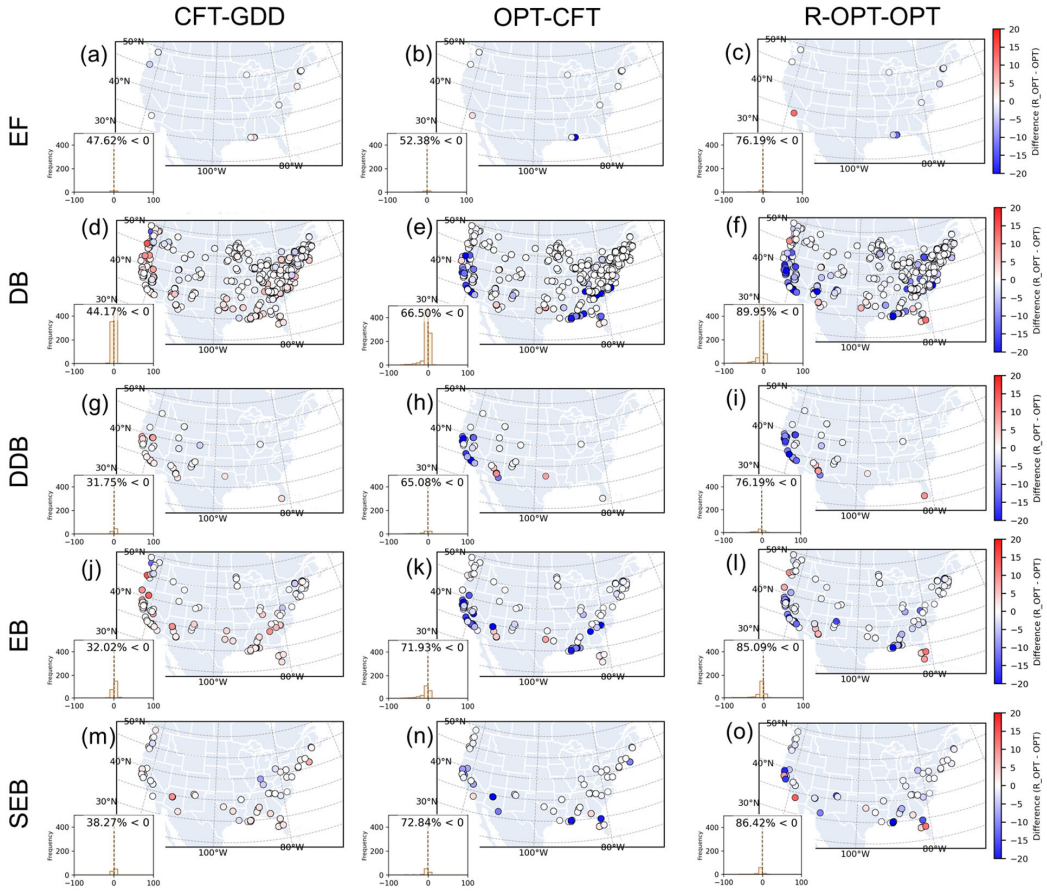


Figure 5. Paired RMSE differences between prognostic models (CFT vs. GDD, OPT vs. CFT, and R-OPT vs. OPT) for five plant functional types: EF (**a**–**c**), DB (**d**–**f**), DDB (**g**–**i**), EB (**j**–**l**) [43], and SEB (**m**–**o**). Red color denotes improvements and blue color denotes degradation.

From a functional-type perspective, certain vegetation groups exhibited mixed responses, where model refinements occasionally led to performance declines. For instance, in deciduous broadleaf (DB) forests, the improvement proportion was 44.17% for CFT–GDD (Figure 5d) but increased to 66.50% for OPT–CFT (Figure 5e); in evergreen broadleaf (EB) forests, the respective proportions were 32.02% (CFT–GDD; Figure 5j) and 71.93% (OPT–CFT; Figure 5k). These patterns suggest that while the R-OPT and OPT models generally outperform earlier formulations, the degree of improvement varies across vegetation types and spatial locations, reflecting the heterogeneous environmental conditions across the study region.

3.3. Examining the Importance of Random Forest Factor

Upon analyzing the distribution of parameter *a* across the study region, we generally observed that *a* tends to be larger in areas closer to the equator. Compared to GDD and CFT models, the OPT and R-OPT models, which incorporate optimal theory and plant photosynthetic efficiency, generally exhibit smaller values of *a* (Figure 6a–d). Using a random forest approach to assess the relative importance of environmental factors on *a*, we found that AccumForcing remained the most influential factor (GDD: 69.3%; CFT: 55.2%; OPT: 45.3%; R-OPT: 49.3%), followed by elevation (GDD: 13.5%; CFT: 24.5%; OPT: 25.1%; R-OPT: 14.4%). In contrast, the importance of AccumChilling was lower (GDD: 11.9%; CFT: 12.1%; OPT: 11.1%; R-OPT: 8.4%). Notably, when the R-OPT model incorporated plant photosynthesis, the importance of Aleaf increased, surpassing that of elevation and AccumChilling, reaching 16.1% (Figure 6e–h).

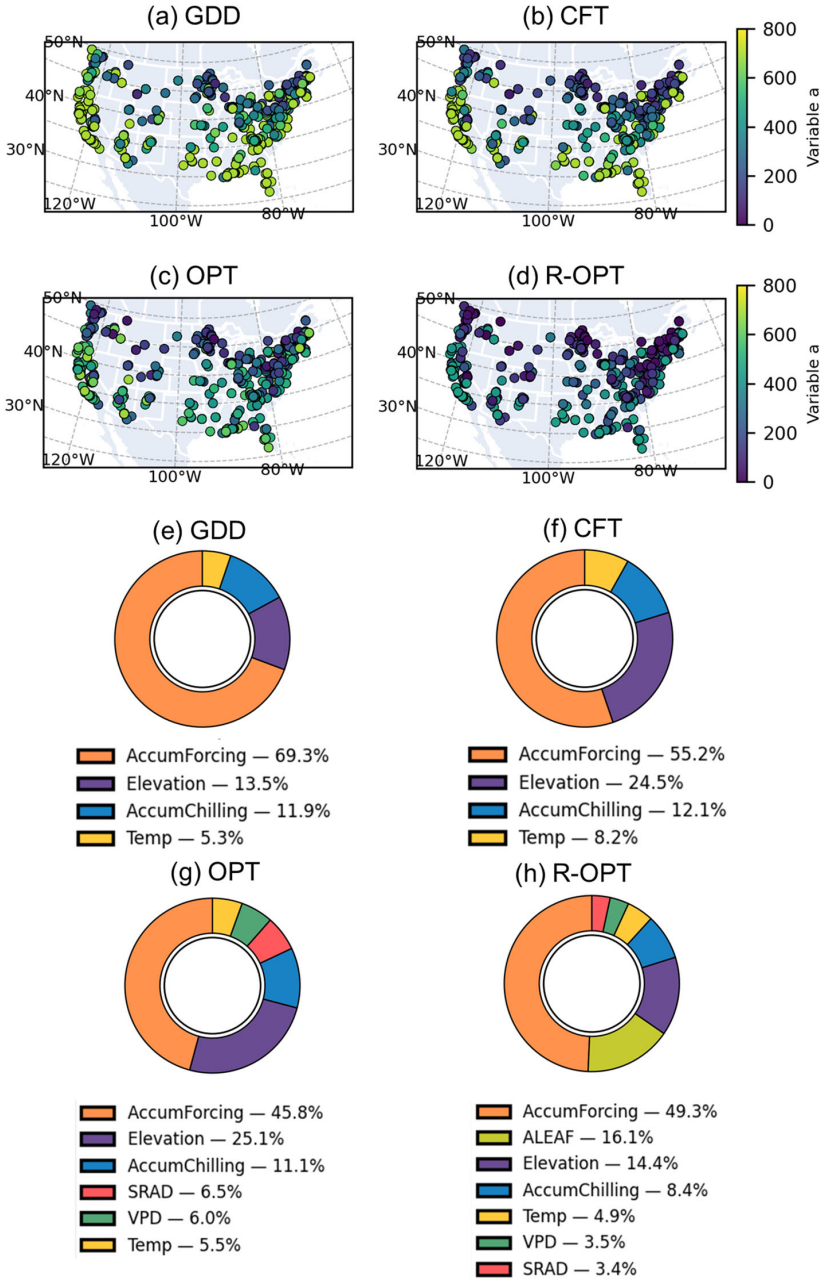


Figure 6. Assessment of the trade-off parameter a distribution across the United States for the four models (GDD, CFT, OPT, R-OPT; **a**–**d**) and Random Forest analysis showing variable contributions to Leaf Unfolding Date (LUD; **e**–**h**).

4. Discussion

In this study, we applied a revised optimality-based spring phenology model (R-OPT) that explicitly integrates the Farquhar–Medlyn photosynthesis framework into the classic OPT structure. Mechanistically, this integration allows leaf-out timing to be constrained not only by thermal cues but also by carbon assimilation capacity, thereby linking phenological decisions to the physiological trade-off between carbon gain and frost risk. Such a formulation is particularly relevant across heterogeneous environments, where photosynthetic capacity and climate jointly regulate plant growth strategies. Building on this mechanistic foundation, our cross-model evaluation across diverse PFTs and sites in the United States demonstrated that R-OPT consistently outperformed three widely used prognostic models—GDD, CFT, and OPT. In terms of predictive accuracy, R-OPT achieved the lowest RMSE (13.11 days; Figure 2). While an average error of approximately two weeks indicates

that considerable uncertainty remains at the site–year scale, this magnitude is comparable to the natural interannual variability of leaf-out dates reported for many temperate PFTs and is therefore acceptable for regional-scale phenological applications. Although R-OPT exhibited a moderately higher AIC than GDD and CFT, the improved accuracy suggests a reasonable trade-off between increased model complexity and predictive performance. Importantly, these improvements were robust across both aggregated analyses and plant functional type-specific evaluations (Figures 3 and 5), highlighting the general applicability of R-OPT in capturing spring phenological dynamics. Nevertheless, even for the best-performing model, a substantial fraction of phenological variability remained unexplained, with R^2 values of approximately 0.40 for deciduous broadleaf PFTs. This residual variance likely reflects site-specific adaptations, intraspecific genetic variability, and unmeasured environmental drivers such as microclimatic heterogeneity, soil moisture dynamics, or photoperiod sensitivity. Residual patterns further indicate that prediction errors are not purely random, suggesting systematic biases at certain sites or years that are not fully captured by the current model structure. It should be noted that the R-OPT framework is intended for regional- to continental-scale phenological analyses and comparative model evaluation, rather than precise prediction at the level of individual PFTs or single sites. The model is designed to capture first-order physiological controls on phenology across broad environmental gradients, which is particularly relevant for large-scale applications and Earth System Model development.

4.1. Model Performance Incorporating Photosynthetic Mechanisms

Differences across Plant Functional Types (PFTs) further revealed ecological insights. evergreen forbs and deciduous broadleaf PFTs showed relatively lower RMSEs compared with other PFTs, whereas drought-deciduous broadleaf PFTs exhibited larger uncertainties. However, the extremely large RMSE values observed for drought-deciduous broadleaf (DDB), evergreen broadleaf (EB), and semi-evergreen broadleaf (SEB) PFTs—exceeding 50 days in some cases—indicate substantial limitations in model applicability for these PFTs. Relatively high RMSE values for some plant functional types mainly reflect strong biological heterogeneity, data limitations, and broad spatial aggregation, rather than deficiencies of the R-OPT framework itself. Such errors are expected in large-scale phenological analyses and might be interpreted in relation to the intended model scope. In particular, drought-deciduous PFTs often rely primarily on water availability [44,45] and soil moisture pulses rather than temperature or carbon gain to regulate leaf phenology, which violates key assumptions shared by R-OPT and other tested models [46]. These results suggest that carbon- and temperature-based phenology models may be insufficient for water-limited functional types without explicit representation of hydrological controls [47–49], which could be further enhanced by incorporating explicit water-stress controls (e.g., precipitation) while disentangling their shared variability to avoid multicollinearity among water-limiting factors as well as PFT-specific dormancy and chilling–forcing dynamics to further reduce prediction errors [17,50]. Spatial patterns in model performance shed further light on the mechanisms underlying phenological control. R-OPT improvements over OPT were clearest at low-altitude sites ($\leq$1000 m) environments (Figure 4). At the same time, the apparent superior performance of R-OPT at high elevations (>2000 m) should be interpreted cautiously, as these elevation classes contain fewer observations, which may reduce variability and inflate performance metrics. Nonetheless, the consistent relative improvement of R-OPT over simpler models across elevation bands suggests that the observed pattern cannot be fully attributed to sampling bias alone. In such settings, plant carbon gain is strongly regulated by temperature and water availability, making the mechanistic treatment of photosynthesis particularly beneficial [20,51,52]. Meanwhile, in high elevation

areas, the forest cover is much smaller than in low elevation areas, underscoring that the added physiological mechanisms remain relevant across diverse environments [53]. Forest cover in these regions is typically sparse, and plant communities often exhibit reduced biodiversity and narrower thermal tolerances. Such characteristics can heighten plant sensitivity to temperature variability, making phenological responses more directly tied to environmental constraints [54].

The observed spatial patterns in model improvement are not random but instead reflect systematic differences in climatic, topographic, and vegetation characteristics across the study region. Sites showing consistent improvement of R-OPT over OPT are predominantly located in coastal and high-latitude regions, where phenological timing is strongly constrained by temperature and growing-season length, and where integrating photosynthetic carbon gain provides additional predictive power. In contrast, sites exhibiting performance degradation are more frequently found in regions characterized by stronger water limitation or mixed climatic controls, where phenology is less directly linked to temperature-driven photosynthesis. These spatial contrasts suggest that R-OPT performs best in environments where carbon assimilation and thermal constraints jointly regulate spring phenology, whereas its advantages diminish in systems dominated by hydrological or disturbance-driven controls.

4.2. Environmental and Trait Controls on the Trade-Off Parameter a

Analysis of model parameters offered mechanistic clarity on these spatial and PFT-specific patterns. The latitudinal gradient in parameter a, with larger values near the equator, aligns with known geographic variation in thermal and photoperiodic constraints on phenology. Compared with GDD and CFT, the optimality-based OPT and R-OPT models estimated generally smaller a values, reflecting their ability to incorporate physiological efficiency rather than relying solely on thermal summation. Random forest analyses further identified accumulated forcing as the strongest predictor of a, followed by elevation, whereas accumulated chilling showed limited influence. Notably, once photosynthesis was explicitly included in R-OPT, Aleaf emerged as a dominant driver (Figure 6), rather than treating phenology as only temperature- or chilling-driven [9,55]. This highlights the central role of leaf-level carbon assimilation traits in determining phenological timing and supports the mechanistic value of incorporating photosynthetic constraints [56,57]. This finding indicates that many current models may systematically underestimate the contribution of plant functional traits to phenological variability, particularly across PFT assemblages or biomes with diverse leaf economic strategies [58,59]. Incorporating these traits, therefore, not only improves predictive skill, but also enhances the biological interpretability of model behavior—an essential step toward process-based forecasts under future climate conditions [60].

4.3. Implications of the Findings

Together, these results hold important implications for large-scale phenology modeling and Earth System Models [61,62]. Because spring phenology regulates the onset of carbon uptake and transpiration, improved predictions can enhance simulation of ecosystem carbon and water fluxes [2,63]. While model parsimony is often prioritized in ESM applications to ensure computational efficiency and parameter identifiability, our results indicate that incorporating key physiological processes—such as mechanistic representations of photosynthesis—can substantially improve predictive skill without incurring prohibitive complexity. The strong performance of R-OPT demonstrates that coupling phenology with mechanistic photosynthesis enhances the ecological realism of model predictions across climatic gradients [9,64]. Furthermore, the spatial variability identified in model performance emphasizes the need

to account for environmental heterogeneity, PFT-specific strategies, and local trait variation when scaling phenological processes to regional and global applications.

The R-OPT framework presents important strengths, while several limitations remain. Firstly, R-OPT assumes relatively static trait values (e.g., A_{leaf}), yet leaf economic traits often vary within PFTs across environmental gradients or shift plastically in response to nutrient availability, light conditions, or prior-year carbon balance [65,66]. However, our empirical analyses indicate that optimized A_{leaf} values exhibit no pronounced systematic variation across either interannual timescales or broad spatial (latitudinal) gradients within the study domain, suggesting that A_{leaf} can be reasonably treated as a quasi-static trait in the present application. Without accounting for trait plasticity, ontogenetic variation, or acclimation, the model may underestimate phenological variability in heterogeneous or rapidly changing environments [67,68]. Secondly, the model's performance across scales warrants further evaluation. R-OPT remains primarily validated at plot and site scales; its behavior under large spatial scaling, interannual climate extremes, or future climate scenarios is still insufficiently tested. Thirdly, there might be elevation mismatches between observation sites and grid cell centers for some environmental variables. Future research should expand cross-biome validation, integrate additional environmental constraints, refine trait parameterization using broader datasets, and examine how R-OPT scales across temporal and spatial domains to improve its generalizability and predictive robustness [20,69]. Explicit sensitivity analyses that relax the assumption of trait stationarity would further strengthen future applications of the model. Nevertheless, the R-OPT framework does not explicitly represent all potential drivers of vegetation phenology [70–72], such as photoperiod constraints, carbon storage dynamics, or disturbance effects. As a result, its predictive performance may be limited under extreme climatic events or in ecosystems where additional controls play a dominant role [73].

Overall, our study demonstrates that R-OPT provides a mechanistically grounded, empirically validated, and broadly robust framework for predicting spring phenology. By directly linking phenological timing to photosynthetic processes, the model advances understanding of PFT-specific adaptive strategies and strengthens the foundation for improved ecosystem modeling and climate impact assessment.

5. Conclusions

In conclusion, our study demonstrates that integrating mechanistic photosynthesis into an optimality-based spring phenology model substantially improves predictive accuracy and robustness across PFTs, environmental gradients, and functional types. The R-OPT model consistently outperforms traditional GDD and CFT models, as well as the original OPT model, while capturing key interspecific differences in phenological strategies. Our findings highlight the critical role of photosynthetic processes, thermal forcing, and site-specific environmental factors in regulating spring leaf-out, providing a mechanistic basis for phenology modeling. By linking phenological timing to carbon gain–chilling risk trade-offs, the R-OPT model offers a more generalizable and mechanistically grounded framework, with important implications for improving ecosystem and Earth System Models. Future studies incorporating additional physiological traits, climate extremes, and PFT interactions will further enhance our understanding of spring phenology and its responses to global environmental change.

Supplementary Materials: The following supporting information can be downloaded at: https://www.mdpi.com/article/10.3390/f17020287/s1, Table S1: The formula of four representative spring phenology models. For abbreviation letters in "Input" aspect: T, temperature responses are not separable in chilling or forcing; C, chilling temperature; F, forcing temperature; P, photo-period;

and G, carbon gain responses by photosynthesis. The mathematical formula is provided in the Supplementary Materials.

Author Contributions: Y.G. conceived the study and performed the analyses. Y.G., Q.W., X.W. and Y.W. designed the analyses. All authors contributed to interpreting the results. Y.G., Q.W., X.W. and Y.W. drafted the manuscript, and all authors contributed to the manuscript editing. All authors have read and agreed to the published version of the manuscript.

Funding: This work was supported by the Basic Research Program of Jiangsu Province for Young Scientists (#BK20251471), the Fundamental Research Funds for the Central Universities (#B250201125), the General Program of National Natural Science Foundation of China (#525037811), National Natural Science Foundation of China (#42401450).

Data Availability Statement: The data that support the findings of this study are available from the corresponding author upon reasonable request.

Conflicts of Interest: Yantian Wang is employed by NARI Group Corporation State Grid, Electric Power Research Institute, Nanjing NARI Information Communication Technology Co., Ltd., Nanjing, China; his employer's company was not involved in this study, and there is no relevance between this research and their company.

References

1. Flynn, D.F.B.; Wolkovich, E.M. Temperature and photoperiod drive spring phenology across all species in a temperate forest community. *New Phytol.* **2018**, *219*, 1353–1362. [CrossRef] [PubMed]
2. Gu, H.; Qiao, Y.; Xi, Z.; Rossi, S.; Smith, N.G.; Liu, J.; Chen, L. Warming-induced increase in carbon uptake is linked to earlier spring phenology in temperate and boreal forests. *Nat. Commun.* **2022**, *13*, 3698. [CrossRef] [PubMed]
3. Zheng, J.; Xu, X.; Jia, G. Effects of shifting spring phenology on growing season carbon uptake in high latitudes. *J. Geophys. Res. Biogeosciences* **2022**, *127*, e2022JG006900. [CrossRef]
4. Ma, X.; Zhu, X.; Xie, Q.; Jin, J.; Zhou, Y.; Luo, Y.; Liu, Y.; Tian, J.; Zhao, Y. Monitoring nature's calendar from space: Emerging topics in land surface phenology and associated opportunities for science applications. *Glob. Change Biol.* **2022**, *28*, 7186–7204. [CrossRef]
5. Lamichhane, J.R. Rising risks of late-spring frosts in a changing climate. *Nat. Clim. Change* **2021**, *11*, 554–555. [CrossRef]
6. Liu, Y.; Liu, X.; Fu, Z.; Zhang, D.; Liu, L. Soil temperature dominates forest spring phenology in China. *Agric. For. Meteorol.* **2024**, *355*, 110141. [CrossRef]
7. Silvestro, R.; Deslauriers, A.; Prislan, P.; Rademacher, T.; Rezaie, N.; Richardson, A.D.; Vitasse, Y.; Rossi, S. From Roots to Leaves: Tree Growth Phenology in Forest Ecosystems. *Curr. For. Rep.* **2025**, *11*, 12. [CrossRef]
8. Chen, L.; Peñuelas, J. Ecosystem Phenology: Integrating Traits and Processes Beyond Observable Events. *Glob. Change Biol.* **2025**, *31*, e70480. [CrossRef]
9. Wang, J.; Hua, H.; Guo, J.; Huang, X.; Zhang, X.; Yang, Y.; Wang, D.; Guo, X.; Zhang, R.; Smith, N.G.; et al. Late spring frost delays tree spring phenology by reducing photosynthetic productivity. *Nat. Clim. Change* **2025**, *15*, 201–209. [CrossRef]
10. Chang, Q.; Ficklin, D.L.; Jiao, W.; Denham, S.O.; Wood, J.D.; Brunsell, N.A.; Matamala, R.; Cook, D.R.; Wang, L.; Novick, K.A. Earlier ecological drought detection by involving the interaction of phenology and Eco-Physiological function. *Earth's Future* **2023**, *11*, e2022EF002667. [CrossRef]
11. Rauschkolb, R.; Herben, T.; Kattge, J.; Knickmann, B.; Linstädter, A.; Menzel, A.; Mora, K.; Nordt, B.; Vitasse, Y.; Weigelt, P. The performance of growing degree day models to predict spring phenology of herbaceous species depends on the species' temporal niche. *Funct. Ecol.* **2025**, 1–14. [CrossRef]
12. Chamberlain, C.; Wolkovich, E. Variation across space, species and methods in models of spring phenology. *Clim. Change Ecol.* **2023**, *5*, 100071. [CrossRef]
13. Van de Vijver, E.; Landschoot, S.; Smagghe, G.; De Baets, B.; Temmerman, F.; Dillen, J.; Haesaert, G. Potentials and limitations of a growing degree day approach to predict the phenology of cereal leaf beetles. *Environ. Entomol.* **2018**, *47*, 1039–1046. [CrossRef] [PubMed]
14. Schädel, C.; Seyednasrollah, B.; Hanson, P.J.; Hufkens, K.; Pearson, K.J.; Warren, J.M.; Richardson, A.D. Using long-term data from a whole ecosystem warming experiment to identify best spring and autumn phenology models. *Plant-Environ. Interact.* **2023**, *4*, 188–200. [CrossRef] [PubMed]
15. Mo, Y.; Li, X.; Guo, Y.; Fu, Y. Warming increases the differences among spring phenology models under future climate change. *Front. Plant Sci.* **2023**, *14*, 1266801. [CrossRef]

16. Li, S.; Wang, Y.; Ciais, P.; Sitch, S.; Sato, H.; Shen, M.; Chen, X.; Ito, A.; Wu, C.; Kucharik, C.J. Deficiencies of phenology models in simulating spatial and temporal variations in temperate spring leaf phenology. *J. Geophys. Res. Biogeosci.* **2022**, *127*, e2021JG006421. [CrossRef]
17. Luedeling, E.; Schiffers, K.; Fohrmann, T.; Urbach, C. PhenoFlex-an integrated model to predict spring phenology in temperate fruit trees. *Agric. For. Meteorol.* **2021**, *307*, 108491. [CrossRef]
18. Hu, Z.; Jin, C.; Peng, S.; Yang, Y.; Yang, G.; Smith, N.G. Simulating climatic responses of vegetation production with ecological optimality theories. *Innov. Geosci.* **2025**, *3*, 100153-1–100153-11. [CrossRef]
19. Gu, Y.; Meng, L.; Wang, Y.; Wu, Z.; Pan, Y.; Zhao, Y.; Detto, M.; Wu, J. Uncovering the role of solar radiation and water stress factors in constraining decadal intra-site spring phenology variability in diverse ecosystems across the Northern Hemisphere. *New Phytol.* **2025**, *246*, 1986–2003. [CrossRef]
20. Gu, Y.; Wu, Z.; Detto, M.; Yang, D.; Wang, J.; Zhao, Y.; Yang, X.; Wu, J. Improving leaf spring phenology modelling for temperate tree species: An integration of the Farquhar–Medlyn photosynthesis model with the optimality-based approach. *Methods Ecol. Evol.* **2025**, *16*, 2901–2918. [CrossRef]
21. Chamberlain, C.J.; Wolkovich, E. Late spring freezes coupled with warming winters alter temperate tree phenology and growth. *New Phytol.* **2021**, *231*, 987–995. [CrossRef] [PubMed]
22. Grossman, J.J. Phenological physiology: Seasonal patterns of plant stress tolerance in a changing climate. *New Phytol.* **2023**, *237*, 1508–1524. [CrossRef] [PubMed]
23. Ren, P.; Li, P.; Zhou, X.; Liu, Z.; Tang, J.; Zhang, C.; Zou, Z.; Li, T.; Peng, C. Shifts in Plant Phenology Significantly Affect the Carbon Allocation in Different Plant Organs. *Ecol. Lett.* **2024**, *27*, e70024. [CrossRef] [PubMed]
24. Norton, A.J.; Bloom, A.A.; Parazoo, N.C.; Levine, P.A.; Ma, S.; Braghiere, R.K.; Smallman, T.L. Improved process representation of leaf phenology significantly shifts climate sensitivity of ecosystem carbon balance. *Biogeosciences* **2023**, *20*, 2455–2484. [CrossRef]
25. Liu, C.; Peltoniemi, M.; Alekseychik, P.; Mäkelä, A.; Hölttä, T. A Coupled Model of Hydraulic Eco-Physiology and Cambial Growth—Accounting for Biophysical Limitations and Phenology Improves Stem Diameter Prediction at High Temporal Resolution. *Plant Cell Environ.* **2025**, *48*, 1344–1365. [CrossRef]
26. Oliver, R.J.; Mercado, L.M.; Clark, D.B.; Huntingford, C.; Taylor, C.M.; Vidale, P.L.; McGuire, P.C.; Todt, M.; Folwell, S.; Shamsudheen Semeena, V. Improved representation of plant physiology in the JULES-vn5. 6 land surface model: Photosynthesis, stomatal conductance and thermal acclimation. *Geosci. Model Dev. Discuss.* **2022**, *15*, 5567–5592. [CrossRef]
27. Walker, A.P.; De Kauwe, M.G.; Bastos, A.; Belmecheri, S.; Georgiou, K.; Keeling, R.F.; McMahon, S.M.; Medlyn, B.E.; Moore, D.J.; Norby, R.J. Integrating the evidence for a terrestrial carbon sink caused by increasing atmospheric CO_2. *New Phytol.* **2021**, *229*, 2413–2445. [CrossRef]
28. Chen, S.; Liu, D.; Zhang, Y.; Zheng, R.; Wang, T. Data-constrained modeling of terrestrial gross primary production over the Tibetan Plateau for 2003–2019. *Agric. For. Meteorol.* **2024**, *355*, 110129. [CrossRef]
29. Alkama, R.; Forzieri, G.; Duveiller, G.; Grassi, G.; Liang, S.; Cescatti, A. Vegetation-based climate mitigation in a warmer and greener World. *Nat. Commun.* **2022**, *13*, 606. [CrossRef]
30. Thornton, P.; Thornton, M.; Mayer, B.; Wei, Y.; Devarakonda, R.; Vose, R.; Cook, R. Daymet: Daily surface weather data on a 1-km grid for North America, version 3. In *USDA-NASS, 2019. 2017 Census of Agriculture, Summary and State Data, Geographic Area Series, Part 51, AC-17-A*; ORNL DAAC: Oak Ridge, TN, USA, 2016; Volume 51.
31. Taylor, S.D.; Meiners, J.M.; Riemer, K.; Orr, M.C.; White, E.P. Comparison of large-scale citizen science data and long-term study data for phenology modeling. *Ecology* **2019**, *100*, e02568. [CrossRef]
32. Rosemartin, A.H.; Denny, E.G.; Gerst, K.L.; Marsh, R.L.; Posthumus, E.E.; Crimmins, T.M.; Weltzin, J. *USA National Phenology Network Observational Data Documentation*; 2331-1258; US Geological Survey: Reston, VA, USA, 2018.
33. de la Torre Cerro, R.; Holloway, P. A review of the methods for studying biotic interactions in phenological analyses. *Methods Ecol. Evol.* **2021**, *12*, 227–244. [CrossRef]
34. Zhao, Y.; Diao, C.; Augspurger, C.K.; Yang, Z. Monitoring spring leaf phenology of individual trees in a temperate forest fragment with multi-scale satellite time series. *Remote Sens. Environ.* **2023**, *297*, 113790. [CrossRef]
35. Griffith, G. Level III North American Terrestrial Ecoregions: United States Descriptions. *Prep. North Am. Comm. Environ. Coop.* **2010**, 1–64.
36. Chen, J.M.; Wang, R.; Liu, Y.; He, L.; Croft, H.; Luo, X.; Wang, H.; Smith, N.G.; Keenan, T.F.; Prentice, I.C.; et al. Global datasets of leaf photosynthetic capacity for ecological and earth system research. *Earth Syst. Sci. Data* **2022**, *14*, 4077–4093. [CrossRef]
37. Meng, L.; Zhou, Y.; Gu, L.; Richardson, A.D.; Peñuelas, J.; Fu, Y.; Wang, Y.; Asrar, G.R.; De Boeck, H.J.; Mao, J.; et al. Photoperiod decelerates the advance of spring phenology of six deciduous tree species under climate warming. *Glob. Change Biol.* **2021**, *27*, 2914–2927. [CrossRef]
38. Wang, H.; Wu, C.; Ciais, P.; Peñuelas, J.; Dai, J.; Fu, Y.; Ge, Q. Overestimation of the effect of climatic warming on spring phenology due to misrepresentation of chilling. *Nat. Commun.* **2020**, *11*, 4945. [CrossRef]

39. Gu, Y.; Zhao, Y.; Guo, Z.; Meng, L.; Zhang, K.; Wang, J.; Lee, C.K.; Xie, J.; Wang, Y.; Yan, Z. The underappreciated importance of solar radiation in constraining spring phenology of temperate ecosystems in the Northern and Eastern United States. *Remote Sens. Environ.* **2023**, *294*, 113617. [CrossRef]
40. Farquhar, G.D.; von Caemmerer, S.v.; Berry, J.A. A biochemical model of photosynthetic CO_2 assimilation in leaves of C3 species. *Planta* **1980**, *149*, 78–90. [CrossRef]
41. Medlyn, B.E.; Duursma, R.A.; Eamus, D.; Ellsworth, D.S.; Prentice, I.C.; Barton, C.V.; Crous, K.Y.; De Angelis, P.; Freeman, M.; Wingate, L. Reconciling the optimal and empirical approaches to modelling stomatal conductance. *Glob. Change Biol.* **2011**, *17*, 2134–2144. [CrossRef]
42. Yates, L.A.; Aandahl, Z.; Richards, S.A.; Brook, B.W. Cross validation for model selection: A review with examples from ecology. *Ecol. Monogr.* **2023**, *93*, e1557. [CrossRef]
43. Liu, Q.; Fu, Y.H.; Zeng, Z.; Huang, M.; Li, X.; Piao, S. Temperature, precipitation, and insolation effects on autumn vegetation phenology in temperate China. *Glob. Change Biol.* **2016**, *22*, 644–655. [CrossRef] [PubMed]
44. White, M.A.; Thornton, P.E.; Running, S.W. A continental phenology model for monitoring vegetation responses to interannual climatic variability. *Glob. Biogeochem. Cycles* **1997**, *11*, 217–234. [CrossRef]
45. Li, H.L.; Ali, A.; Luo, X.; Liao, K.; Sun, N.; Xu, M.S.; Sha, L.B.; He, D.; Du, Y.J.; Sun, W.W. China's subtropical deciduous plants are more sensitive to climate change than evergreen plants by flowering phenology. *Glob. Change Biol.* **2024**, *30*, e17168. [CrossRef]
46. Caldararu, S.; Purves, D.W.; Smith, M.J. The effect of using the plant functional type paradigm on a data-constrained global phenology model. *Biogeosciences* **2016**, *13*, 925–941. [CrossRef]
47. Plos, C.; Hensen, I.; Korell, L.; Auge, H.; Römermann, C. Plant species phenology differs between climate and land-use scenarios and relates to plant functional traits. *Ecol. Evol.* **2024**, *14*, e11441. [CrossRef]
48. König, P.; Tautenhahn, S.; Cornelissen, J.H.C.; Kattge, J.; Bönisch, G.; Römermann, C. Advances in flowering phenology across the Northern Hemisphere are explained by functional traits. *Glob. Ecol. Biogeogr.* **2018**, *27*, 310–321. [CrossRef]
49. Asse, D.; Randin, C.F.; Bonhomme, M.; Delestrade, A.; Chuine, I. Process-based models outcompete correlative models in projecting spring phenology of trees in a future warmer climate. *Agric. For. Meteorol.* **2020**, *285–286*, 107931. [CrossRef]
50. Vitasse, Y.; Signarbieux, C.; Fu, Y.H. Global warming leads to more uniform spring phenology across elevations. *Proc. Natl. Acad. Sci. USA* **2018**, *115*, 1004–1008. [CrossRef]
51. Chapman, D.S. Greater phenological sensitivity to temperature on higher Scottish mountains: New insights from remote sensing. *Glob. Change Biol.* **2013**, *19*, 3463–3471. [CrossRef]
52. Richardson, A.D.; Friedland, A.J. A Review of the Theories to Explain Arctic and Alpine Treelines Around the World. *J. Sustain. For.* **2009**, *28*, 218–242. [CrossRef]
53. Sun, Y.; Guan, Q.; Du, Q.; Wang, Q.; Sun, W. Elevation dependence of vegetation growth stages and carbon sequestration dynamics in high mountain ecosystems. *Environ. Res.* **2025**, *273*, 121200. [CrossRef] [PubMed]
54. He, H.; Moore, T.; Lafleur, P.; Sonnentag, O.; Humphreys, E.; Wu, M.; Roulet, N. Spring phenology in photosynthesis control and modeling for a temperate bog. *Front. Environ. Sci.* **2025**, *13*, 1548578. [CrossRef]
55. Peng, Y.; Li, P.; Zhou, X.; Luo, Y.; Zhang, C.; Wang, L.; Li, T.; Peng, C. Divergent contributions of spring and autumn photosynthetic phenology to seasonal carbon uptake of subtropical vegetation in China. *J. Geogr. Sci.* **2024**, *34*, 1280–1296. [CrossRef]
56. Zohner, C.M.; Renner, S.S.; Sebald, V.; Crowther, T.W. How changes in spring and autumn phenology translate into growth-experimental evidence of asymmetric effects. *J. Ecol.* **2021**, *109*, 2717–2728. [CrossRef]
57. Luo, Y.; Zohner, C.; Crowther, T.W.; Feng, J.; Hoch, G.; Li, P.; Richardson, A.D.; Vitasse, Y.; Gessler, A. Internal physiological drivers of leaf development in trees: Understanding the relationship between non-structural carbohydrates and leaf phenology. *Funct. Ecol.* **2024**, 1–14. [CrossRef]
58. Sporbert, M.; Jakubka, D.; Bucher, S.F.; Hensen, I.; Freiberg, M.; Heubach, K.; König, A.; Nordt, B.; Plos, C.; Blinova, I. Functional traits influence patterns in vegetative and reproductive plant phenology–a multi-botanical garden study. *New Phytol.* **2022**, *235*, 2199–2210. [CrossRef]
59. Navarro, T.; Hidalgo-Triana, N. Variations in leaf traits modulate plant vegetative and reproductive phenological sequencing across arid Mediterranean shrublands. *Front. Plant Sci.* **2021**, *12*, 708367. [CrossRef]
60. Kanta, C.; Kumar, A.; Chauhan, A.; Singh, H.; Sharma, I.P. The Interplay Between Plant Functional Traits and Climate Change. In *Plant Functional Traits for Improving Productivity*; Kumar, N., Singh, H., Eds.; Springer Nature: Singapore, 2024; pp. 41–58.
61. Li, X.; Ault, T.; Richardson, A.D.; Carrillo, C.M.; Lawrence, D.M.; Lombardozzi, D.; Frolking, S.; Herrera, D.A.; Moon, M. Impacts of shifting phenology on boundary layer dynamics in North America in the CESM. *Agric. For. Meteorol.* **2023**, *330*, 109286. [CrossRef]
62. Chen, M.; Melaas, E.K.; Gray, J.M.; Friedl, M.A.; Richardson, A.D. A new seasonal-deciduous spring phenology submodel in the Community Land Model 4.5: Impacts on carbon and water cycling under future climate scenarios. *Glob. Change Biol.* **2016**, *22*, 3675–3688. [CrossRef]

63. Teets, A.; Bailey, A.S.; Hufkens, K.; Ollinger, S.; Schädel, C.; Seyednasrollah, B.; Richardson, A.D. Early spring onset increases carbon uptake more than late fall senescence: Modeling future phenological change in a US northern deciduous forest. *Oecologia* **2023**, *201*, 241–257. [CrossRef]
64. Fang, J.; Shugart, H.H.; Wang, L.; Lutz, J.A.; Yan, X.; Liu, F. Optimal representation of spring phenology on photosynthetic productivity across the northern hemisphere forests. *Agric. For. Meteorol.* **2024**, *350*, 109975. [CrossRef]
65. Wang, H.; Prentice, I.C.; Wright, I.J.; Warton, D.I.; Qiao, S.; Xu, X.; Zhou, J.; Kikuzawa, K.; Stenseth, N.C. Leaf economics fundamentals explained by optimality principles. *Sci. Adv.* **2023**, *9*, eadd5667. [CrossRef] [PubMed]
66. Li, Y.; Liu, C.; Sack, L.; Xu, L.; Li, M.; Zhang, J.; He, N. Leaf trait network architecture shifts with species-richness and climate across forests at continental scale. *Ecol. Lett.* **2022**, *25*, 1442–1457. [CrossRef] [PubMed]
67. De Lisle, S.P.; Mäenpää, M.I.; Svensson, E.I. Phenotypic plasticity is aligned with phenological adaptation on both micro-and macroevolutionary timescales. *Ecol. Lett.* **2022**, *25*, 790–801. [CrossRef] [PubMed]
68. Burton, T.; Ratikainen, I.I.; Einum, S. Environmental change and the rate of phenotypic plasticity. *Glob. Change Biol.* **2022**, *28*, 5337–5345. [CrossRef]
69. Pawar, S.; Huxley, P.J.; Smallwood, T.R.; Nesbit, M.L.; Chan, A.H.; Shocket, M.S.; Johnson, L.R.; Kontopoulos, D.-G.; Cator, L.J. Variation in temperature of peak trait performance constrains adaptation of arthropod populations to climatic warming. *Nat. Ecol. Evol.* **2024**, *8*, 500–510. [CrossRef]
70. Forsythe, W.C.; Rykiel, E.J., Jr.; Stahl, R.S.; Wu, H.-i.; Schoolfield, R.M. A model comparison for daylength as a function of latitude and day of year. *Ecol. Model.* **1995**, *80*, 87–95. [CrossRef]
71. De Réaumur, R. Observations du thermomere. *Mem. Acad. R. Sci. Paris* **1735**, 545–576.
72. Hänninen, H. Modelling bud dormancy release in trees from cool and temperate regions. *Acta For. Fenn.* **1990**, *213*, 1–47.
73. Li, D.; Belitz, M.; Campbell, L.; Guralnick, R. Extreme weather events have strong but different impacts on plant and insect phenology. *Nat. Clim. Change* **2025**, *15*, 321–328. [CrossRef]

Disclaimer/Publisher's Note: The statements, opinions and data contained in all publications are solely those of the individual author(s) and contributor(s) and not of MDPI and/or the editor(s). MDPI and/or the editor(s) disclaim responsibility for any injury to people or property resulting from any ideas, methods, instructions or products referred to in the content.